

A Transient Unified Model of Arc-Weld Pool Couplings during Pulsed Spot Gas Tungsten Arc Welding

A. Traidia^{1,2}, F. Roger^{*1}

¹ENSTA Paristech, Department of Mechanics UME

²AREVA NP, Technical Center

*Corresponding author: ENSTA Paristech, Department of Mechanics UME, Chemin de la hunière, 91761 Palaiseau , FRANCE, frederic.roger@ensta-paristech.fr

Abstract: A transient finite element model has been developed to study the heat transfer and fluid flow during pulsed spot GTA welding on stainless steel. Temperature field, fluid velocity and electromagnetic fields are computed inside the cathode, arc-plasma and anode using a unified MHD formulation. The evolution of the heat flux and current density at the top surface of the anode are studied during the welding process. The electric heating flux at the anode which represents the energy absorbed by the workpiece from the electrons coming from the cathode is found to be the major mechanism of heating. The proposed numerical model also permits to study the time evolution of the weld pool dimensions for both constant and pulsed current. A comparison shows that the use of a pulsed current welding gives a wider and deeper weld shape than the mean constant current welding. The present work lays a foundation for the future development of a three-dimensional model for moving torch arc welding.

Keywords: Heat transfer, Fluid flow, Arc-plasma, Unified model, Marangoni effect.

1. Introduction

Due to the widespread use of GTA welding in the manufacturing industry, the numerical simulation of such a process is currently in great progress. The main goal is to study the impact of the welding parameters (welding current, arc length, pulse frequency, welding speed ...) on the final weld shape in order to improve the welding quality and increase productivity. The complexity of the numerical modeling is due the strong couplings between many physics involved in this process. The ionization of the shielding gas ensures the current flow between the two electrodes, then the heating Joule effect creates a thermal plasma composed of electrons, ions and neutral species at a large temperature range; from 300 K to more than 20 000 K. The workpiece is

then heated from both the arc-plasma conduction, and the electrons flow at the top surface. Depending on the melting temperature of the workpiece, a weld pool is formed in which the fluid flow is governed by the Marangoni effect at the top surface, the buoyancy forces and the electromagnetic forces created by the current flow. The fluid flow inside the weld pool is also strongly coupled to the temperature field and the deformation of the top free surface.

Many numerical models of spot GTAW are available in the literature [1-5]. Most of them consider only one part of the welding process [1-4] (either the cathode, or the arc plasma, or the anode) which leads to fix some boundary conditions that do not represent the real situations. The best way to deal with the problem is to take into account the three parts (anode, cathode and arc-plasma) in a unified formalism. The interfaces between the plasma and the electrodes are then considered as internal boundaries. This approach was proposed by Lowke and Tanaka *et al* [5] and gives satisfying results for constant current welding.

In the present work, a unified finite element model is introduced taking into account the three parts of the welding process. The time-dependent model can simulate pulsed current welding in which the welding current varies with time at a given frequency between two constant values; the peak current and the background current. This permits to study the transient evolution of some physical quantities at the transition between the peak and background times but also to compare welding under pulsed current with welding under the mean corresponding constant current.

2. Mathematical formulation

1.1 Governing equations

The mathematical formulation is based on the following assumptions:

- The study is restricted to spot GTAW; an axisymmetric coordinate system is used.
- The arc column is assumed to be pure argon at Local Thermodynamic Equilibrium.
- The gas plasma and molten metal are incompressible.
- A weak coupling is considered between the free surface deformation and the Magneto Hydrodynamic (MHD) calculations.

The temperature, velocity and pressure fields are calculated in the three domains using the classical conservation equations written in a unified transient formalism as follows:

(1) *Conservation of mass*

$$\nabla \cdot \vec{v} = 0$$

(2) *Conservation of momentum*

$$\rho \left(\frac{\partial \vec{v}}{\partial t} + \vec{v} \cdot \nabla \vec{v} \right) = -\nabla p + \mu \nabla \cdot (\nabla \vec{v} + \nabla \vec{v}^T) + \vec{j} \times \vec{B} + \rho \vec{g} (1 - w_p \beta (T - T_{ref}))$$

(3) *Conservation of energy*

$$\rho c_p^{eq} \left(\frac{\partial T}{\partial t} + \vec{v} \cdot \nabla T \right) = \nabla \cdot (k \nabla T) + \vec{j} \cdot \vec{E} + \frac{5k_B}{2e} \vec{j} \cdot \nabla T - 4\pi \varepsilon_N (1 - w_p)$$

Where \vec{v} is velocity, T is temperature, p is pressure, ρ is density, $c_p^{eq} = c_p + w_p L_f \frac{df_L}{dT}$ is an

equivalent specific heat that takes into account the latent heat of fusion L_f , f_L is the liquid fraction assumed to vary linearly with temperature in the mushy zone and w_p equals 1 in the weld pool and 0 elsewhere. k is thermal conductivity and μ is the viscosity. The Boussinesq approximation is used to compute the convection forces inside the weld pool. β is the metal thermal expansion and T_{ref} is taken as the solidus temperature.

In the weld pool the volumetric heat source is the Joule effect and the enthalpic flux, and in the arc plasma we take in addition the radiation losses, usually approximated by $4\pi \varepsilon_N$, where ε_N is the

net emission coefficient of argon that varies with temperature.

The determination of the electromagnetic forces and the joule effect in both arc plasma and work piece requires the computation of the current density \vec{j} and the magnetic flux \vec{B} . To achieve this, the coupled current continuity and the magnetic potential equations are computed as function of the electric potential V and the magnetic potential vector \vec{A} as follows:

$$\nabla \cdot \left(\sigma \nabla V + \sigma \frac{\partial \vec{A}}{\partial t} \right) = 0$$

$$\sigma \frac{\partial \vec{A}}{\partial t} + \nabla \times \left(\frac{1}{\mu_0} \nabla \times \vec{A} \right) + \sigma \nabla V = \vec{0}$$

The current density, electric field and magnetic flux are then computed from V and \vec{A} as follows:

$$\vec{E} = -\nabla V - \frac{\partial \vec{A}}{\partial t}; \quad \vec{j} = -\sigma \nabla V - \sigma \frac{\partial \vec{A}}{\partial t}; \quad \vec{B} = \nabla \times \vec{A}$$

It is important to notice that the eddy current $\vec{j}_e = -\sigma \frac{\partial \vec{A}}{\partial t}$ created by the time variation of the welding current is taken into account in the above expressions.

The free surface deformation $\varphi(r)$ is described by the following PDE obtained from [2]:

$$P_a - \rho g \varphi - \lambda = -\gamma \frac{r \varphi_{rr} + \varphi_r (1 + \varphi_r^2)}{r (1 + \varphi_r^2)^{3/2}}$$

Where φ is the free surface depression, Pa is the arc pressure, γ is the molten metal surface tension and λ is a Lagrangian multiplier used to take into account the mass conservation constraint: $\int 2\pi \varphi(r) r dr = 0$.

1.2 Boundary conditions

The computational domain is shown in Figure 1. As seen the workpiece is made of two subdomains in order to use a finer mesh size for the weld pool formation. All the boundary conditions are listed in Table 1; the most important points are discussed below;

At the interface between arc plasma and the anode (GD) the following conditions must be satisfied [5]:

$$[-k \nabla T \cdot (-\vec{n})]_{anode} - [-k \nabla T \cdot (-\vec{n})]_{plasma} = |\vec{j} \cdot \vec{n}| \phi_a - \varepsilon \sigma_B T^4$$

$$\mu \frac{\partial (\vec{v} \cdot \vec{s})}{\partial \vec{n}} = \vec{\tau}_a + f_L \frac{\partial \gamma}{\partial T} \frac{\partial T}{\partial \vec{s}}$$

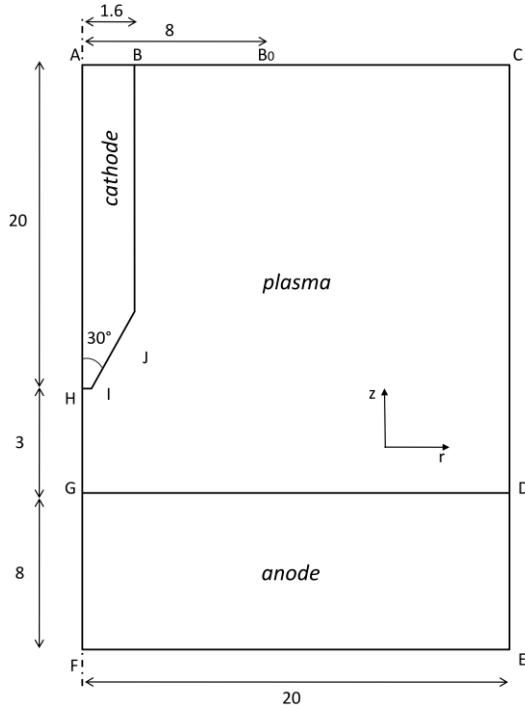


Figure 1. Computational domain (dimensions in mm)

The first condition shows that the normal heat flux at the anode is composed by the heating conduction flux from the plasma, the heating electric flux (which represents the energy transferred from the electrons to the anode) and the cooling radiation losses. ϕ_a is the anode work function and σ_B is the Stefan-Boltzmann constant.

The second condition means that the total shear stress is the sum of the arc drag force and the Marangoni force. \vec{s} and \vec{n} are respectively a local tangent vector and the normal vector to the top free surface (\vec{n} is directed toward the plasma domain). $\partial\gamma/\partial T$ is the surface tension coefficient, which has been reported to have a big impact on the flow directions inside the weld pool [1-4]. Its dependence on temperature T and sulfur activity a_s is considered using the expression developed by Sahoo and DebRoy *et al* [6] as follows:

$$\frac{\partial\gamma}{\partial T} = -A_\gamma - R_g \Gamma_s \ln(1 + Ka_s) - \frac{Ka_s}{1 + Ka_s} \Gamma_s \frac{\Delta H_0}{T}$$

$$K(T) = k_1 \exp\left(-\frac{\Delta H_0}{R_g T}\right)$$

Along the interface between the arc plasma and the cathode (HIJB), the normal discontinuity of the heat flux is expressed as follows:

$$[-k\nabla T \cdot (-\vec{n})]_{cathode} - [-k\nabla T \cdot (-\vec{n})]_{plasma} = j_i V_i - j_e \phi_c - \varepsilon \sigma_B T^4$$

Where V_i and ϕ_c are respectively the argon ionization potential and the cathode work function. j_i and j_e are respectively the ion current and electron current calculated from:

$$j_e = j_r \cdot \left[(|\vec{j} \cdot \vec{n}| - j_r) > 0 \right] + |\vec{j} \cdot \vec{n}| \cdot \left[(|\vec{j} \cdot \vec{n}| - j_r) < 0 \right]$$

$$j_i = |\vec{j} \cdot \vec{n}| - j_e$$

$$j_r = A_r T^2 \exp\left(\frac{-e\phi_e}{k_B T}\right)$$

A_r , ϕ_e and e are respectively the Richardson's constant, the effective work function for thermionic emission and the elementary charge.

Table 1: Boundary conditions

AB	$T = T_0; \vec{j} \cdot \vec{n} = \frac{I(t)}{\pi R_c^2}$
BB₀	$T = T_0; \vec{v} \cdot \vec{n} = -Ug\alpha z; \vec{j} \cdot \vec{n} = 0; \vec{A} \times \vec{n} = 0$
B₀C CD	$T = T_0; \vec{j} \cdot \vec{n} = 0; p = p_0;$ $\vec{n} \cdot \underline{\underline{\tau}} \cdot \vec{n} = 0; \vec{A} \times \vec{n} = \vec{0}$
DE EF	$\vec{q} \cdot \vec{n} = h_c(T - T_0); \vec{v} = \vec{0}; V = 0; \vec{A} \times \vec{n} = 0$
FA	$\vec{q} \cdot \vec{n} = 0; \vec{v} \cdot \vec{n} = 0; \vec{j} \cdot \vec{n} = 0; \vec{B} = \vec{0}$
GD	$[-k\nabla T \cdot (-\vec{n})]_{anode} - [-k\nabla T \cdot (-\vec{n})]_{plasma} = \vec{j} \cdot \vec{n} \phi_a - \varepsilon \sigma_B T^4$ $\mu \frac{\partial(\vec{v} \cdot \vec{s})}{\partial \vec{n}} = \vec{\tau}_a + f_e \frac{\partial\gamma}{\partial T} \frac{\partial T}{\partial \vec{s}}$ $\vec{v} \cdot \vec{n} = 0; \ \vec{j} \cdot \vec{n}\ = 0$
HB	$[-k\nabla T \cdot (-\vec{n})]_{cathode} - [-k\nabla T \cdot (-\vec{n})]_{plasma} = j_i V_i - j_e \phi_c - \varepsilon \sigma_B T^4$ $\vec{v} = \vec{0}; \ \vec{j} \cdot \vec{n}\ = 0$

3. Numerical simulation results

The numerical model is applied to an AISI 304 stainless steel disk containing 290 ppm sulfur with 8 mm thickness. The thermophysical properties of AISI 304 ss are listed in the appendix. The properties of pure argon are taken from [7]. The gas inflow rate is fixed to 30 L/min. Table 2 lists the other welding parameters.

Table 2: Welding parameters

Peak current	160 A
Background current	80 A
Peak pulse duration	0.5 s
Frequency	1 Hz
Total heating time	15 s

Figure 2 presents the time evolution of the computed solution at the end of the background time (left) and the peak time (right) every five periods. It is represented the temperature field and temperature contours inside the arc plasma and the electrode, the normalized velocity field and streamlines inside the molten weld pool.

During the peak time the arc is bell-shaped and the maximum of temperature and velocity fields are higher than during the background time. The obtained values for the maximum of plasma-jet velocity and plasma temperature are in good agreement with the literature, in fact for a 150 A continuous current welding 17000 K for the maximum temperature and 150 m/s for the maximum velocity are reviewed [5]. We can also notice that the variations of temperature and velocity fields inside the plasma column between the peak times are negligible; this is also the case for the background times.

The dynamic of the weld pool flow is studied by considering the streamlines of the velocity field. We can clearly identify in each figure two vortices named A and B. They result from the Marangoni effect at the top surface of the weld pool, the size of each vortex is related to both temperature distribution at the surface and sulfur content of the workpiece. Details about the dynamic variation of these vortices and their influence on the weld pool evolution are available in our previous works [4].

Figure 3 shows the anodic heat flux distribution during the transition from the last peak time ($t=14.5$ s) to the last peak time (15 s). During the background time the maximum of anodic flux is around 43 W/mm^2 . The transition is then very fast; in approximately $15 \mu\text{s}$ the heat flux seems to stabilize especially at the center of the disk and reaches a maximum of 56.6 W/mm^2 .

The numerical model permits to study the energy transfer between the arc plasma and the workpiece. Figure 4 shows the radial evolution of the heat flux at the anode at the last peak and background times ($t=14.5$ s and $t=15$ s). In each figure it is represented the total heat flux and its elementary contributions, namely; the electric flux $|\vec{j} \cdot \vec{n}| \phi_a$, the conduction from the arc plasma $[-k \nabla T \cdot \vec{n}]_{plasma}$ and the radiation losses $\varepsilon \sigma_B T^4$.

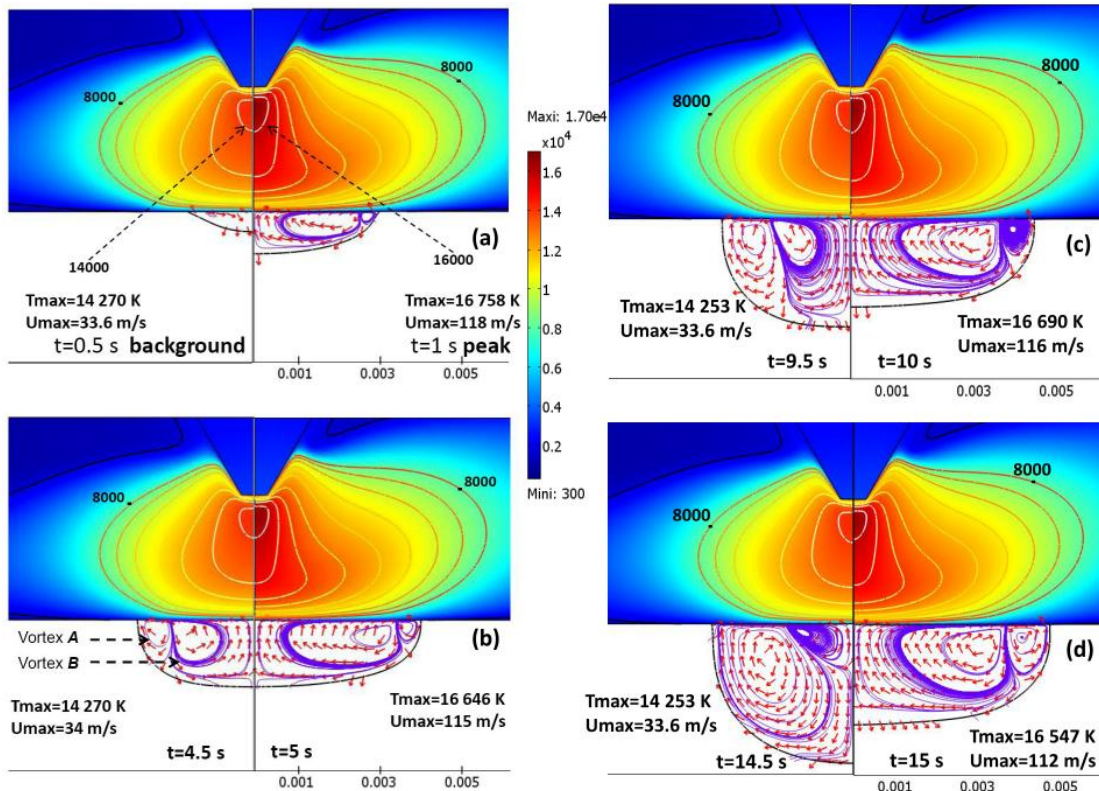


Figure 2. MHD solutions at background times (left) and peak times (right) for different periods

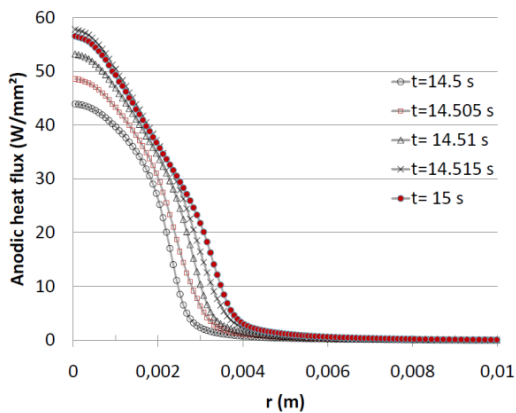


Figure 3. Evolution of the anodic heat flux at the transition between the background to the peak time

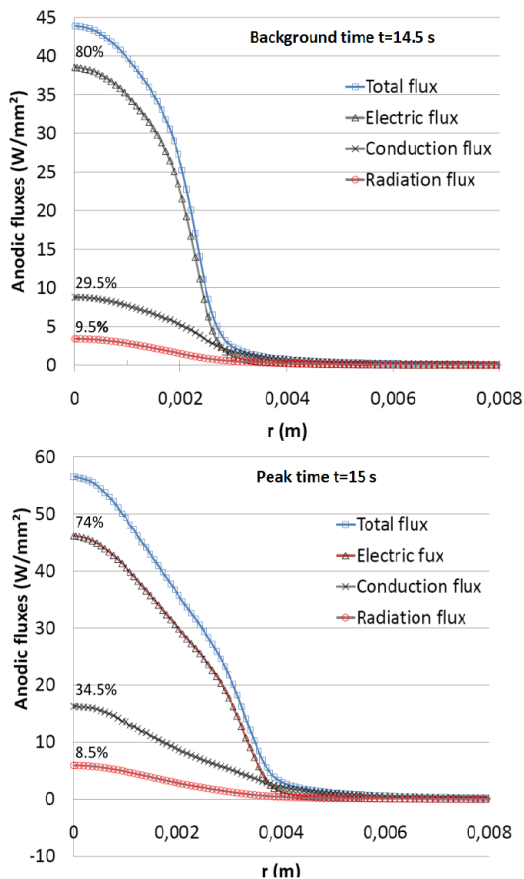


Figure 4. Anodic heat flux and its elementary contributions at the last period of heating

The electric flux is found to be the most significant factor in both peak and background times. It represents around 80 % of the total

energy transferred to the workpiece. The contribution of the conductive heat flux from the plasma represent around 30 % and the cooling radiation losses are under 10 % of the total heat flux.

Figure 5 shows the time evolution of the weld pool half-width and depth for the pulsed current 80/160 A and the continuous mean current 120 A. Even though the two cases are energetically equivalent, the pulsed case produces a deeper and wider weld pool than the continuous case, especially for the weld pool depth. This conclusion goes with what is commonly observed by welders.

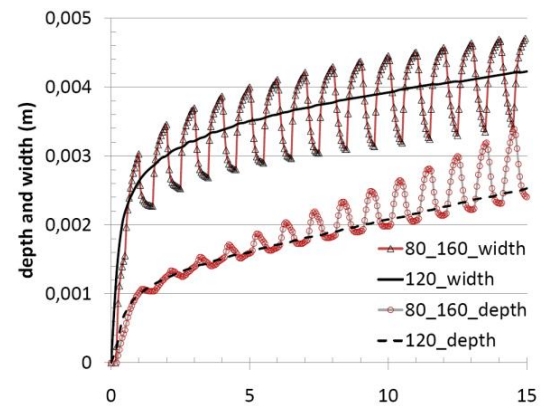


Figure 5. Evolution of the weld pool size for the pulsed current 80/160 A and the mean current 120 A

4. Conclusions

A transient unified model of pulsed spot GTAW has been developed using COMSOL Multiphysics. The numerical simulation allowed a better understanding of the heat transfer between the arc plasma and the electrodes. The heating thermionic emission at the anode was found to be the most important heating effect. The results showed that for a given level of energy, it is more interesting to use a pulsed current welding than the mean constant current to get a better weld size.

8. References

1. W.H. Kim and S.J. Na. *Int. J. Heat Mass Tran.* , **41**, 3213-3227 (1998)
2. H.G. Fan, H.L. Tsai and S.J. Na. *Int. J. Heat Mass Tran.* , **44**, 417-428 (2001)

3. F. Lu, S. Yao, S. Lou and Y. Li. *Comput. Mater. Sci.*, **29**, 371-378 (2004)
4. A. Traidia, F. Roger and E. Guyot. *Int. J. Therm. Sci.*, **49**, 1197-1208 (2010)
5. M. Tanaka and J.J. Lowke. *J. Phys. D: Appl. Phys.*, **40**, R1-R23 (2007)
6. P. Sahoo, T. DebRoy, M.T. McNallan. *Metall. Trans. B.*, **19B**, 483-491 (1988)
7. P. Fauchais, M. Boulos and E. Pfender, *Thermal plasma, fundamentals and applications*, (1994)

9. Acknowledgements

This research was supported by the Technical Center of welding at AREVA NP, FRANCE. The authors are grateful to Lahcene Cherfa, Alexander Chidley and Catherine Holm for their help on the results processing.

Appendix

Table 3: Material properties of the used materials.

ρ	6080 to 7272 $kg.m^{-3}$
c_p	510 to 796 $J.kg^{-1}.K^{-1}$
k	15.2 to 42.8 $W.m^{-1}.K^{-1}$
μ	0.05 $kg.m^{-1}.s^{-1}$
σ	$7.7 \times 10^5 \Omega^{-1}.m^{-1}$
T_l	1723 K
T_s	1673 K
a_s	0.029 wt%
A_γ	$4.3 \times 10^{-4} N.m^{-1}.K^{-1}$
R_g	8314 $J.kg^{-1}.mole^{-1}.K^{-1}$
ΔH_0	$-1.66 \times 10^8 J.kg^{-1}.mole^{-1}$
Γ_s	$1.3 \times 10^{-8} J.kg^{-1}.mole^{-1}.m^{-2}$
γ_m	1.943 $N.m^{-1}$
ϕ_a	4.65 V
ϕ_c	4.52 V
ϕ_e	2.63 V
h_c	15 $W.m^{-2}.K^{-1}$
ε	0.4